ISBN: 978-3-95450-198-4 doi:10.18429/JACoW-COOL2017-MOA21

EMITTANCE EVOLUTION IN MICE*

M. A. Uchida†, Imperial College London, UK
for the MICE collaboration

Abstract

The Muon Ionization Cooling Experiment (MICE) was designed to demonstrate a measurable reduction in beam emittance due to ionization cooling. The emittance of a variety of muon beams was reconstructed before and after a "cooling cell", allowing the change in the phase-space distribution due to the presence of an absorber to be measured.

The core of the MICE experiment is a cooling cell that can contain a range of solid and cryogenic absorbers inside a focussing solenoid magnet. For the data described here, a single lithium hydride (LiH) absorber was installed and two different emittance beam have been analysed. Distributions that demonstrate emittance increase and equilibrium have been reconstructed, in agreement with theoretical predictions.

Data taken during 2016 and 2017 is currently being analysed to evaluate the change in emittance with a range of absorber materials, different initial emittance beams and various magnetic lattice settings. The current status and the most recent results of these analyses is presented.

INTRODUCTION

The International Muon Ionization Cooling Experiment (MICE) was designed and constructed to demonstrate the process of ioniziation cooling [1], applied to muon beams. It was constructed at the Rutherford Appleton Laboratory, and has been successfully taking data since 2015. Figure 1 shows the total number of integrated event triggers, as a function of time for the current configuration of the experiment.

MICE is a single particle experiment where each event contains a single muon passing through the beamline. Individual muon tracks are then reconstructed in each of the detectors. This data is aggregated at analysis in order to study the evolution of both individual track parameters and ensemble effects, when various absorber materials are placed within the cooling channel.

The primary goal is to measure the phase-space volume of the muon beam before and after a cooling cell by reconstructing the normalised, transverse RMS emittance (referred to simply as "emittance"). This corresponds the volume occupied by the central 68% of a gaussian-distributed ensemble of particles. This is easily calculated by constructing the covariance matrix for an ensemble, Σ, in the position-momentum phase-space, using the variables: x, p_x, y, p_y. The emittance can then be calculated as:

$$\epsilon_\perp = \frac{|\Sigma|^{\frac{1}{4}}}{m}, \qquad (1)$$

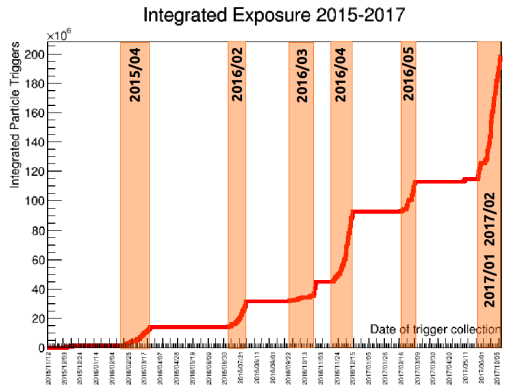

Figure 1: The integrated number of event triggers as a function of time. The ISIS user periods in which MICE is operational are highlighted.

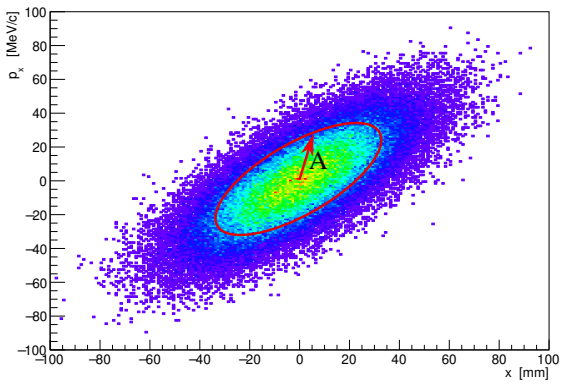

Figure 2: Example phase-space distribution with a contour of equal amplitude marked in red.

where $\epsilon_\perp$ is the emittance, and m is the muon mass.

In order to analyse the effect of a single muon on the evolution of emittance, an additional quantity is defined: the single particle amplitude, $A_\perp$. This corresponds to the scalar distance a given particle is found from the centre of the beam (Figure 2). The definition is weighted by the covariance matrix such that amplitude is invariant under conservative transformations, e.g. focussing. It is defined by,

$$A_\perp = \epsilon_\perp \mathbf{v}^\intercal \Sigma^{-1} \mathbf{v} \qquad (2)$$

where $\mathbf{v} = (x, p_x, y, p_y)$ is the particle's coordinate vector.

The behaviour of the beam emittance in the presence of an absorber material can be approximated by the cooling

* Work supported by the (UK) Science and Technology Facilities Council and the (US) Dept. of Energy and National Science Foundation
† m.a.uchida@imperial.ac.uk

ISBN: 978-3-95450-198-4 doi:10.18429/JACoW-COOL2017-MOA21

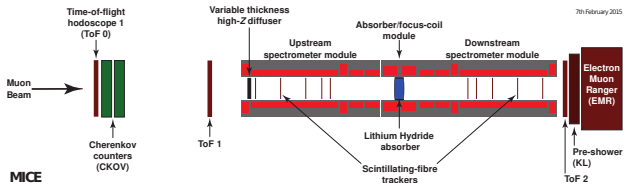

Figure 3: Layout of the MICE experiment in its current configuration. The upstream detectors are illustrated in the order in which the incoming beam crosses them, the solenoid magnet coils are marked in red and the absorber module is shown in blue.

equation,

$$\frac{d\epsilon_\perp}{dx} = -\frac{\epsilon_\perp}{\beta^2 E}\left\langle\frac{dE}{dx}\right\rangle + \frac{\beta_\perp (13.6\,\mathrm{MeV/c})^2}{2\beta^3 E m_\mu X_0}, \qquad (3)$$

which describes the rate of change of emittance with respect to longitudinal position through a material with energy loss, $< dE/dx >$, and radiation length, X_0. β, E and m_μ are the mean relativsitic velocity, energy and mass of the muon beam and $\beta_\perp$ is the betatron function.

THE MICE EXPERIMENT

Transfer Line

The muon beam used by the MICE experiment is produced by dipping a titanium target into the ISIS proton synchrotron. Three triplets of quadrupole magnets provide transverse focussing of the resultant pion and muon beams and a decay solenoid magnet is used to increase the capture efficiency of muons produced from pion decay (Figure 4).

Momentum selection is performed using two dipole magnets, the first selects the pion momentum before decay, and the second selects the resultant muon momentum. This allows for precise control over the final ratio between pions, muons and electrons that enter the cooling channel.

The final component, the variable beam diffuser, is found at the entrance to the cooling channel and is comprised of two brass and two tungsten irises that can diffuse the incoming muon beam via multiple Coulomb scattering. This provides a method to vary the intial beam emittance before entering the cooling channel.

Diagnostics

A range of diagnostic detectors [2] are installed in order ensure that the species of particle can be precisely determined. Muons are selected with a high efficiency upstream of the cooling channel, and any muons that decay can be tagged downstream of the cooling channel.

Upstream, aerogel-based cerenkov detectors provide coarse velocity measurements and are used in conjunction with time-of-flight counters that identify muons, pions and electrons by their transit time between fixed points.

Downstream of the cooling channel, a third time-of-flight counter is used in addition to the Kloe-light (KL) and

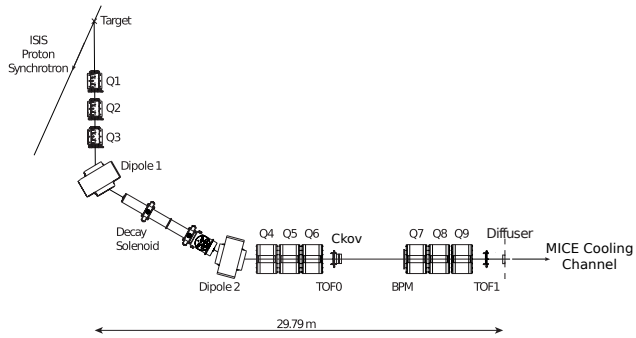

Figure 4: Layout of the transfer line from the ISIS synchrotron through to the MICE Cooling Channel.

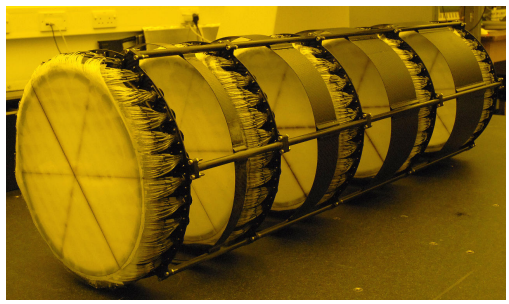

Figure 5: Photograph of a scintillating fibre tracker under construction. The yellow light was required in order to prevent damage the fibres.

electron-muon ranger (EMR) calorimeters. The combination of precise time-of-flight measurements, and the identification of stopped particle tracks in the calorimetry systems, allows for better than 99% muon identification [3].

The Trackers

The primary detectors used in the reconstruction of emittance are the scintillating fibre trackers [4]. They consist of five stations, which are in turn composed of the 3 planes of 350 μm scintillating fibres. This allows for a position resolution better than 0.5 mm, and a transverse momentum resolution of approximately 1 MeV/c [5].

The fibres are read out using visual light photon counters (VLPCs) and processed to reconstruct position where overlapping channels are found across all three planes for a given station. This triplet requirement results in a noise rejection of better than 99.9%.

A Kalman filter based track fitting routine performs the final track fit for each tracker and allows precise determination of the track parameters at a reference plane. The reference plane for each tracker is defined as the plane that is closest to the absorber. This provides the nominal position at which results for different settings and configurations may be compared.

Optics

The MICE cooling channel (illustrated in Figure 3), is composed of three solenoid magnets: spectrometer solenoid-upstream (SSU), absorber focus coil (AFC), and spectrome-

ISBN: 978-3-95450-198-4 doi:10.18429/JACoW-COOL2017-MOA21

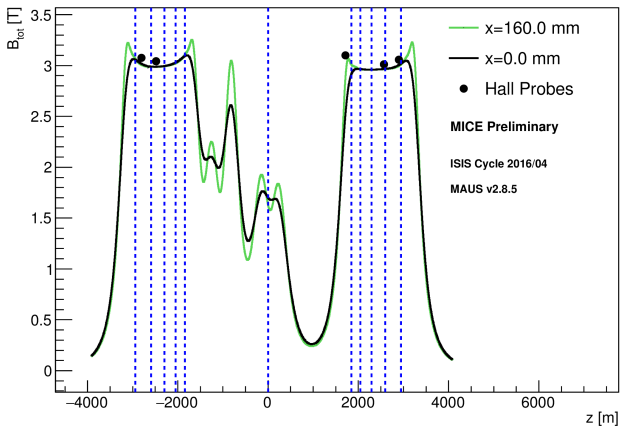

Figure 6: Magnetic field configuration of the MICE cooling channel in solenoid mode. The black line shows the mean, on-axis field and the green shows the mean field strength at the radius of the hall probe locations. Black points show the respective values from the hall probes within the magnet bore.

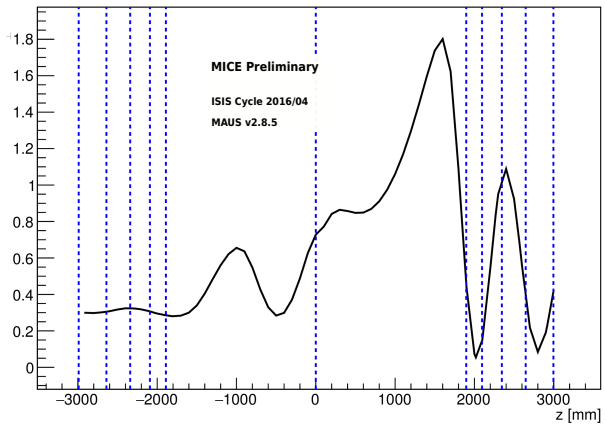

Figure 7: The betatron function from simulation for the magnetic configuration that was used during data taking. The blue dashed lines highlight the positions of the 5 tracker stations, upstream and downstream, in addition to the centre of the LiH absorber.

ter solenoid-downstream (SSD). The LiH absorber is located in the center of the AFC and the individual magnet coils are shown in red.

For the data discussed here, the two matching coils within SSD (those closest to the absorber) were not powered due to concerns over the quench protection system and related hardware issues. They have since been operated succesfully.

The magnetic configuration of the channel that was used during data taking of the emittance-evolution data set is shown in Figure 6. A comparison between the model and hall probe measurements indicates that there is a small systematic error in the magnitude of the estimated field, the effective error of which was estimated using simulation data (section).

Figure 6 also highlights the regions where there are significant field gradients, notably at $z = 1000$ mm, the location of the unpowered downstream match coils. The combination of large betatron function (the transverse extent of the beam) and high field gradient is believed to cause filementation within the beam (where different momentum muons are focussed by different amounts), leading to an apparent emittance growth.

The betatron function, estimated using simulation, is shown in Figure 7. Although well constrained in the upstream portion of the cooling channel, significant oscillations were present due the lack of focussing from the downstream match coils. The matching was optimised using a genetic algorithm to ensure good transmission through to the downstream tracking region, whilst maintaining the betatron function through the absorber.

ANALYSIS PROCEDURE

Event Selection

Each detector was read out and processed using specialised algorithms designed around the physical hardware. The resultant reconstructed spacepoints and tracks were then analysed and selected.

Individual events were primarily selected based on the time-of-flight between TOF0 and TOF1, the chi-squared per degree of freedom of the fitted upstream track and the momentum reconstructed at the reference plane of the upstream tracker. This provided a high-purity ensemble of muons that were well reconstructed by the trackers, with minimal statistical bias in the resultant measurement.

In order to validate the reconstruction of the time-of-flight and tracking detectors, the reconstructed momentum within the upstream tracker was plotted against the reconstructed time-of-flight of each muon entering the cooling channel that passed the selection criteria. The result is shown in Figure 8 and demonstrates very good agreement between the data and theoretical prediction (for the muon mass) shown by the red dashed line.

Additional statistical quantities were used to discriminate against bad events. Primarily, the reconstructed chi-squared value per degree of freedom, χ^2_{NDF}, for the trackers. Events with $\chi^2_{NDF} > 5$ were excluded (both upstream and downstream) as this demonstrates a sub-optimal fit. This rejected less than 1% of potential events and was primarily due to rare hard-scatter events, in which a significant deflection in the track path is observed.

The event selection proceedure was applied only to the upstream tracker, such that the result was unbiased by the preferential selection of events (that would demonstrate cooling). Events that scrape, i.e. interact with the apertures between modules or scatter into a magnet bore, were higher-amplitude particles. Hence, any selection based only on the particles that were transmitted would bias the resultant measurement towards those events that showed a net decrease in amplitude.

ISBN: 978-3-95450-198-4 doi:10.18429/JACoW-COOL2017-MOA21

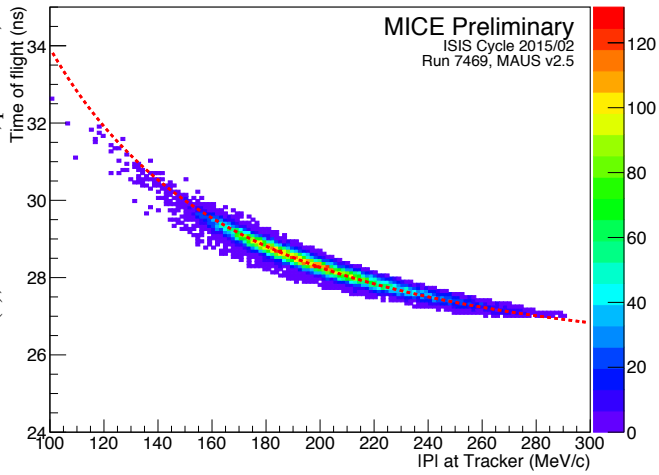

Figure 8: Comparison of the time of the flight between TOF0 and TOF1 and the momentum reconstructed within the upstream tracker. The red dashed line describes the theoretical results for a particle with the muon mass.

Amplitude Reconstruction

For each event that passed the selection criteria (outlined above), the position and momentum components (x, p_x, y, p_y) were reconstructed at the reference plane of the upstream tracker. Similarly, each event for which an upstream track was found and transmitted through to the downstream tracker was reconstructed at the downstream reference plane.

For those events where a track was not located in the downstream tracker, the track was assumed to have been scraped out of the beam and therefore not included in the downstream reconstruction. Such events were flagged and reconstructed as an additional ensemble in the upstream tracker, such that the amplitude distribution of the scraped events could be compared against those that were transmitted.

At each of the upstream and downstream reference planes, the tracks that were selected were used to calculate the beam emittance and amplitude distribution using Equations (1) and (2) respectively.

The statistical error on the emittance was calculated using:

$$\sigma_{\epsilon_\perp} = \frac{\epsilon_\perp}{\sqrt{2(N-1)}} \tag{4}$$

where N is the number of events in the ensemble and $\sigma_{\epsilon_\perp}$ is the standard error on the emittance. The results were used to estimate the statistical error for each bin in amplitude.

The systematic errors were estimated using a Monte Carlo simulation in which each tracker was analysed independently. A realistic reproduction of the data was performed starting from a model of the target. The momentum distributions were tuned to match those of the reconstructed data such that a accurate representation of the experiment was produced.

The simulated data was reconstructed such that for each bin in amplitude, the migration of events that were mis-reconstructed could be calculated. That is the number of events which should have been reconstructed in a given bin, but were found in another bin. This is due to the intrisic statistical precision of the trackers coupled with non-uniformities in the magnetic field.

Each bin in amplitude was then corrected according to the results of the model, and the associated errors were calculated.

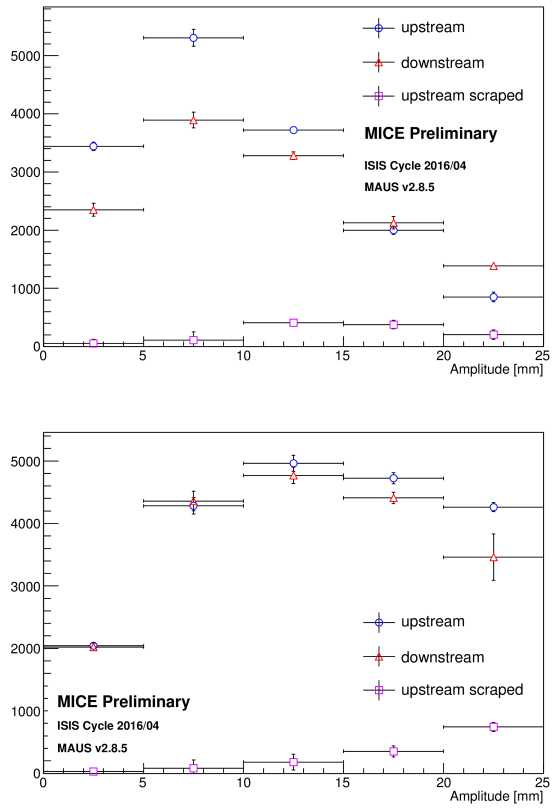

Figure 9: A comparison between the upstream and downstream amplitude distributions for the 3 mm nominal beam and the 6 mm nominal beam. The particles that were reconstructed upstream but were scraped before reaching the downstream tracker are also shown.

EMITTANCE EVOLUTION

The single particle amplitude for each muon was reconstructed for each of the upstream, downstream and scraped ensembles. Two different initial beams were studied: a 3 mm nominal emittance beam and a 6 mm nominal emittance beam. The resultant amplitude distributions are shown in Figure 9.

The region of interest is the core of the beam, where the effects of filementation and scraping are weakest, which is well represented by the first bin in amplitude.

The result for the 3 mm nominal emittance shows a clear reduction within the first bin, significantly above any scaping effects, which is characteristic of an emittance growth i.e. heating. This is in agreement with predictions as lower emittance beam are more difficult to cool, in that they require

ISBN: 978-3-95450-198-4 doi:10.18429/JACoW-COOL2017-MOA21

greater focussing and relative energy losses to acheive the same effect as a larger emittance beam.

The 6 mm result shows very little change between the upstream and downstream reconstruction in the first bin. The neighbouring bins are also consistant and no change within the effects of scraping and the statistical errors is observed. This demonstrates that the net movement of high amplitude particles to lower amplitude is approximately balanced by the net movement of low amplitude particles to higher amplitude. This is consistant with the expected equilibrium emittance for the cooling channel in this configuration at 6 mm.

CONCLUSIONS

The first data for the study of emittance evolution through a LiH absorber has been taken and analysed. A muon beam sample has been selected and reconstructed for two different nominal beam emittances: 3 mm and 6 mm. The distributions of single particle amplitude have been produced and compared, resulting in effects consistent with emittance increase (for the nominal 3 mm beam) and emittance equilibrium (for the nominal 6 mm beam).

Monte Carlo simulations were used in order to validate the reconstruction and analysis techniques, in addition to modelling the errors present in the amplitude distributions. The results were used to estimate the error for each bin in the amplitude distributions.

An additional 10 mm nominal beam is currently being analysed and initial indications show that this setting will demonstrate an increase in amplitude density at the core of the beam, a signal consistent with emittance reduction.

REFERENCES

[1] A. N. Skrinsky *et al.*, “Cooling methods for beams of charged particle,” *Sov. J. Part. Nucl.*, vol. 12, no. 223, 1981.

[2] D. Orestano, “The detector system of the MICE experiment,” *Nucl. Inst. Phys.* A, vol. 617, pp. 45 – 47, 2010.

[3] A. Dobbs *et al.*, “The reconstruction software for the mice scintillating fibre trackers,” *Journal of Instrumentation*, vol. 11, no. 12, p. T12001, 2016.

[4] C. Pidcott, "Multiple scattering and particle identification in the Muon Ionisation Cooling Experiment," PhD thesis, University of Warwick, 2017.

[5] M. Ellis *et al.*, “The design, construction and performance of the MICE scintillating fibre trackers,” *Nuclear Instruments and Methods in Physics Research Section A: Accelerators, Spectrometers, Detectors and Associated Equipment*, vol. 659, no. 1, pp. 136 – 153, 2011.